ORIGINAL PAPERS

Development and characterisation of an irradiation device for biomedical studies covering the solar spectrum with individual regulated spectral bands

B. Plitta-Michalak[1,4] · N. Stricker[1] · E. Pavez Loriè[2,5] · I. Chen[3] · M. Pollet[2] · J. Krutmann[2] · B. Volkmer[3] · R. Greinert[3] · P. Boukamp[2] · A. Rapp[1]

Abstract

To understand the importance of terrestrial solar exposure on human skin, not only individual spectral components need to be considered in biomedical studies, but also the relevance of the combined action profile of the complete solar spectrum (cSS) must be established. We therefore developed a novel irradiation device that combines the emission of four individual lamps (UVB, UVA, VIS and nIR) to achieve exposure from 280 to 1400 nm with individual controllable lamps. The integrated irradiance of each spectral band is similar to the solar spectrum. The lamps can be utilised individually or in any desired combination. Here we present the design, realisation, and validation of this irradiation device as well as biological results on cellular metabolism (MTT assay), cell cycle alterations, and clonogenic growth in HaCaT cells after exposures to the individual spectral bands as well as their simultaneous combinations. Thereby, we demonstrate that UVB combined with UVA is the main determinant for the metabolic activity within cSS. Also, UVB-dependent effects dominate cell cycle regulation in cSS, whilst UVA and nIR have little influence. Lastly, also clonogenic growth is dominated by the UVB action profile in cSS, despite nIR showing modulatory activity when applied in combination with UVB. Together, this highlights the regulatory influence of the different spectral bands on the three biological endpoints and demonstrates their modulation when being part of the complete solar spectrum.

Graphical abstract
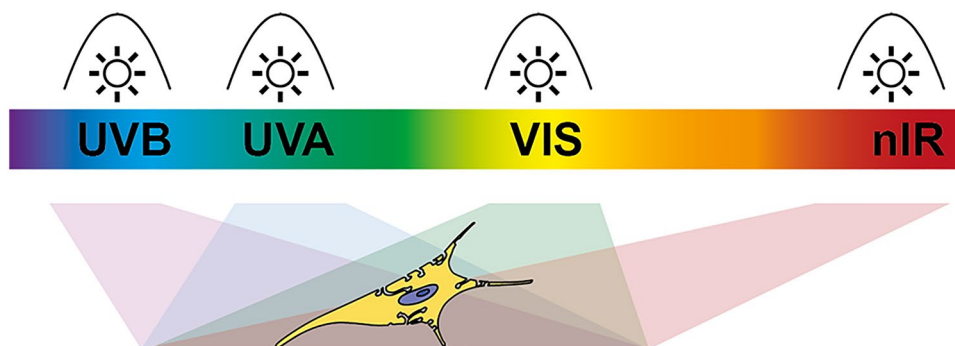
B. Plitta-Michalak and N. Stricker contributed equally.

✉ A. Rapp
  rapp@bio.tu-darmstadt.de

Extended author information available on the last page of the article

1 Introduction

Although there exists overwhelming evidence that UV radiation (280–400 nm), reaching the surface of the earth, is the most important risk factor for skin cancer initiation, the contribution of the different wavelength regions (UVB: 280–315 nm, UVA: 315 − 400 nm) to this development is still poorly understood. Additionally, it is unclear whether the other components of optical radiation, emitted from the sun (visible light (Vis) and near-infrared radiation (nIR)) act synergistically (additively) or, eventually, even in a compensatory way. Indeed, there is no scientific evidence stating that UV exposure is exclusively responsible for skin damage [1]. The historical wavelength bands definitions are not directly related to biological effects, which show a continuous transition. Therefore, this issue needs to be addressed for a correct risk estimation and assessment of terrestrial solar radiation impact on biological systems, as optical radiation qualities are always delivered simultaneously.

Experimental evaluations of the exposure of humans and cultured cell lines to solar radiation have been undertaken for many years. These studies were either performed using individual spectral regions in the UVB or UVA range [2–6] or solar spectrum simulator radiation (SSR) devices were used [7, 8]. The majority of studies using SSR is based on xenon lamps combined with spectral filters to adapt the emission to the solar reference spectrum (air mass filters) [9–11]. The solar spectrum can be mimicked to a good extent (e.g. 0.875–1.125 spectral match in Class A + SSR devices) in a spectral range from 280 to 800 nm and an irradiance of several solar equivalents can be achieved, for studying, e.g. photo-ageing or skin cancer [12]. However, most of devices share the disadvantage of limited emission and missing the typical water absorption bands in the nIR spectral range [13]. Furthermore, the xenon-based SSR devices often have a size-limited homogeneous irradiation area and produce an excessive amount of heat. Recent technological improvements have led to the development of LED-based SSRs [14, 15]. These devices use a combination of individually tuned narrow-banded LEDs to mimic the solar spectrum. Yet, the LED-based SSRs also have some limitations. One important drawback is the low irradiance in the UV (B) and nIR range, due to design limits in the LED substrates. Especially, wavelengths greater than 1100 nm are under-represented and mostly, only the visible spectrum is matched to the reference solar spectrum. Moreover, to perform wavelength-specific exposure (e.g. in the UV wavelength band), the SSR spectrum requires additional filtering, e.g. UG1 filters are introduced to block the visible light spectral components (400–700 nm).

Whilst in conventional SSRs, the spectrum is fixed and can only be altered using specific filters for each specific condition, a device allowing for spectral band-specific irradiation would be desirable. This would allow mimicking different exposure conditions more easily, such as geographical location, ozone layer conditions, season, and effects of sunscreens on different wavelength bands.

Besides improving the area of application, such a device would be suited to also address fundamental radiation biological questions. Accordingly, it is well accepted, and there is ample literature [16–19] reviewed in [20], that the individual spectral bands exhibit different efficacy to induce certain biological effects (e.g. differences in the action spectra for UVB and UVA). In addition, evidence is emerging that the combinations of different spectral bands (e.g. UVB plus UVA, or UVB plus nIR exposure) lead to different biological effects that are not purely additive [21–25]. Therefore, an SSR with tunable spectral bands would be most instrumental for the understanding of solar exposure [26–28].

Here, we describe an SSR that is based on four individual lamps/tubes for the four spectral bands (UVB, UVA, VIS, and nIR), and importantly, which are individually controllable. With biological proof-of-principle experiments, we demonstrate the relevance and practicability of this radiation device, thereby providing first evidence that the combined spectrum (from UVB to nIR) introduces qualitatively and quantitatively different biological effects compared to the different individual wavelength bands.

2 Materials and methods

2.1 Irradiation device

In contrast to existing irradiation sources, where the emission of a single lamp is filtered by appropriate filters [12], the new irradiation device used an additive approach. The part of the solar spectrum in the range of 280–1400 nm is generated by four lamps and combined with dichroic beam combiners onto the sample. Optical filters and dichroic beam combiners control the spectral ranges of the individual lamps. In addition, each lamp is electrically independently switchable and the UVA, UVB, and nIR lamps can be attenuated by specific filters (optical and metal mesh filters) in the corresponding filter sliders. The infrared lamp is additionally filtered by an actively cooled water cuvette and a near-IR-specific band pass filter. The construction of the irradiation device based on four individually controllable lamps is described in detail in the results section. In brief, the cells were irradiated with the following photo-physical conditions: the irradiation area has a size of 17 by 17 cm and thus allows to irradiate five p60 dishes or two 6-well plates simultaneously. The complete base plate of the irradiation device is temperature controlled by Peltier elements to keep the temperature constant.

The standard exposure setting as used in this study provides 0.36 kJ/m^2 UVB, 27.5 kJ/m^2 UVA, 129 kJ/m^2 VIS and 150 kJ/m^2 nIR in approximately 560–630 s, depending on actual lamp output. From these values, the irradiance can be calculated to be approximately 0.64 W/m^2 (UVB), 42 W/m^2 (UVA), 120 W/m^2 (VIS) and 220 W/m^2 (nIR), respectively. The irradiance is measured before each exposure, and the exposure times are adjusted accordingly to compensate, e.g. for lamp ageing. This is achieved by a built-in CCD array spectrometer (Model LR1, Aseq Instruments, Canada), which is fibre-coupled (SMA905) to a cosine adapter located at the centre of the irradiation chamber base plate. This spectrometer allows for every day calibration and compensation of lamp ageing or changes in the spectral composition of the irradiation device. The installed spectrometers were calibrated against a BN 9101 reference lamp (Gigahertz-Optik, Germany) by Photometrik GmbH (Germany). All photometric calculations are performed using a home-made graphical user interface (Processing (www.processing.org)) and the hardware components are controlled through an Arduino micro-computer capable of switching the individual lamps. For each radiation experiment, the user records the actual/current emission spectrum of the lamps using the Aseq software and loads the spectrum into the lamp control software. After providing the set exposure time, the software uses the stored calibration file for the Aseq spectrometer to convert the counts to doses. Then the user sets the desired exposure conditions for each spectral waveband individually and starts the exposure. After the calculated times have been reached, the Arduino microcontroller automatically switches off the respective lamp. An example of the user interface is given in supplementary materials S2.

2.2 Cell culture

HaCaT cells [29] (distributed by CLS Cell lines Service # 300493) were grown in DMEM (4.5 g/L Glucose, L-Glutamine, Sodium pyruvate, 3.7 g/L NaHCO$_3$) (Pan Biotech) containing 10% FBS (Capricorn) and 0.1% Pen/Strep (Pan Biotech) at 37 °C in the presence of 5% CO$_2$. For irradiation, the culture medium was replaced by prewarmed PBS and directly after irradiation, the PBS was changed again to complete culture medium. For cell harvest, HaCaT cells were treated with PBS/EDTA (1 mM) for 2 min followed by Trypsin/EDTA (0.5%/0.2%) for 10 min. Enzymatic activity was stopped by adding 5 mL culture medium and after centrifugation (5 min, 200 g) the single cell suspension was available for further analysis.

2.3 Irradiation

Cells were seeded as described for the individual experiments. The culture medium was replaced by pre-warmed PBS and the cells were irradiated with the indicated doses and spectral combinations. During irradiation (between 10 and 42 min), the temperature of the cells was kept constant at 36 °C by the built-in Peltier element. Temperature was confirmed for several irradiation experiments using a digital temperature probe inserted into the PBS. No significant temperature change was measured during the time of irradiation. Mock-irradiated samples were transferred to PBS and placed inside the irradiation device, but covered in aluminium foil for the same time as the exposed samples. Exposed samples were normalised to the mock-irradiated controls.

2.4 Flow-cytometric quantification of cyclobutane pyrimidine dimers (CPDs)

To compare the biological effects of four similar irradiation devices, located in four different laboratories, we performed a ring trial, relying on flow cytometry-based quantification of UVB and UVA-induced cyclobutane dimers (CPDs). For this, HaCaT cells were irradiated in the individual labs with their respective irradiation devices with increasing doses of UVB (120–288 J/m^2) as well as with one dose of UVA (22 kJ/m^2) and CPD induction was measured in the reference laboratory for all samples simultaneously.

For each measurement, 5×10^5 HaCaT cells were seeded in 60 mm Petri dishes and grown under standard conditions (see above). Cells (in PBS) were exposed to different doses of UVB and UVA at a confluence of 80–90%. Immediately after irradiation, the cells were harvested. The single cells were fixed in 70% ethanol by drop-wise addition to a concentration of 1×10^6 cells/mL and incubated at -20 °C for at least 1 h. Next, 2.5×10^5 cells were permeabilized for 10 min at RT in $1 \times$ blocking and washing solution (Roti®Block, Carl, Roth) with 0.125% Triton X-100. For DNA denaturation, cells were re-suspended in 2 N HCl (Carl Roth) for 10 min at RT followed by a 10 min incubation with 5 μg/mL proteinase K (Sigma) at 37 °C. Cells were incubated with 1 μg/mL mouse anti-CPD antibody (clone KTM53, Kamiya Biomedical Company) overnight at 4 °C. On the next day, cells were incubated with 15 μg/mL goat anti-mouse FITC-conjugated antibody (Dianova) for 1 h at 37 °C and afterwards incubated for 5 min at RT with 10 μg/mL propidium iodide and 0.01% RNase (both from Sigma) prior to measurement with Guava easyCyte 8HT Flow cytometer (Merck).

2.5 MTT assay

To measure cellular metabolism using the MTT assay [30], 1×10^4 HaCaT cells were seeded per well in 4-well plates (2 cm^2 growth area; SPL Life Sciences). Cells were irradiated (in PBS) as indicated in the results section and cultured for the indicated times in regular growth media. Corresponding controls were kept in PBS for the same time as

the irradiated samples. At the time of analysis, the medium was removed and the cells were washed carefully in pre-warmed PBS. Then 1 mL fresh complete culture medium, including MTT at a final concentration of 0.5 mg/mL, was added and the cells were incubated for 2 h at 37 °C. Then 250 µL DMSO were added per well and the formazan was dissolved by shaking on an orbital shaker for 10 min at RT, protected from light. Reduced MTT was measured by absorbance at 590 nm with a reference at 620 nm using a Tecan Infinity M200 plate reader in duplicates per well (technical replicates), and quadruplicates (biological replicates) per condition, resulting in eight measurements per sample. The measurements were normalised to the corresponding control cells.

2.6 Cell cycle analysis

Cell cycle distribution in HaCaT cells following a single exposure as indicated in the results section to individual and combined spectral band irradiation was measured by flow cytometry. For these experiments, we choose a single set of doses (0.36 kJ/m^2 UVB, 27.5 kJ/m^2 UVA, 129 kJ/m^2 VIS and 150 kJ/m^2 nIR), to avoid extensive cell killing (compare Figs. 5A–D). We also omitted VIS exposure on the cell cycle regulation since we did not observe significant effects of VIS in the MTT assay. Cells were seeded in 60 mm dishes and grown to 20% confluency. Then, the cells were irradiated in PBS, fresh culture medium was added and incubated for the indicated times using standard conditions. Thereafter, the cells were harvested by trypsinization and fixed by adding the cell suspension drop-wise into 4.5 mL of ice-cold 70% ethanol. Cells were fixed for at least 2 h at 4 °C. For quantitative DNA staining, the fixed cells were centrifuged (200g, 5 min) and re-suspension in propidium iodide staining solution (0.1% Triton X-100, 0.2 mg/mL RNase A 20 µg/mL propidium iodide in PBS). Cells were incubated at RT for 30 min, followed by overnight incubation at 4 °C, before the cells were analysed for their DNA content using a S3 cell sorter (Biorad) with 488 nm excitation and 615/25 nm emission filters. Cell cycle distributions were quantified using FlowJo (version 10) after doublet discrimination and gating (the gating strategy is depicted in Figure S4) using the Dean–Jett–Fox algorithm. A minimum of four biological replicates were measured per irradiation condition and time point (minimum of 10,000 cells per sample). Statistical testing was performed using one-way ANOVA test. Individual measurements for each irradiation condition and time point were compared for each fitted cell cycle phase to the control measurements separately. Post analysis using Dunnett's post test with a significance level

of 0.05 was used. Significance levels are indicated using * as described in the figure legend.

2.7 Colony formation assay

Five hundred HaCaT cells were seeded in a 60 mm Petri dish (24 cells/cm^2) and cultured overnight at 37 °C. For irradiation, the medium was exchanged to PBS and the cells were irradiated with the indicated spectral bands and doses. Thereafter, the PBS was replaced with culture medium and the cells were incubated for 9 days at 37 °C under standard conditions. Then cells were fixed with 5 mL ice-cold methanol (100%) for 5 min, washed twice with PBS and stained with 5 mL 0.2% methylene blue in methanol (50%) for 10 min at RT. After three washings with ddH$_2$O, the colonies in all individual dishes were counted. Examples of stained colonies are shown in Figure S5. As controlled microscopically, a colony of cells was defined as a cluster of at least 50 normal-sized cells, thereby excluding significant contribution of giant or large multi-nucleated cells. Quantitative analysis of colonies was performed after recoding images of the plates (Amersham AI600 imager) using imageJ. In brief, the images were cropped to the individual dishes, "Auto-threshold (Max Entropy)" was applied and a mask was generated. The mask was processed with a watershed algorithm to separate touching colonies. Then the "Analyze Particles" function was used with the following settings: size: 10–500 pixels, circularity: 0.1–1.0. The results of the automated counted were inspected manually and false detection was corrected. At least four biological replicates were analysed per irradiation condition. The dose–response curves were generated using a linear regression model. Significance of slopes to be non-zero was calculated using F-statistics. Colony sizes were compared using one-way ANOVA test with Bonferroni post test. Colony sizes from one measurement were compared to the matching control. A significance level of 0.05 was used.

3 Results

3.1 Design and construction of a solar spectrum irradiator based on four separate lamps

For the combinatorial irradiation device, the following lamps were chosen: Philips PL-S 9W/12 2P UVB broadband tubes for the UVB range, Philips Cleo high-pressure lamp for the UVA spectral band, and Osram Xenon high-pressure short arc lamp XBO R 300 W/60C OFR for the visible spectrum. For the nIR range, a GE Healthcare 750 W Halogen lamp HPL 750 W LL 240 V was integrated (Fig. 1A). All lamps were equipped with additional reflectors to maximise light output.
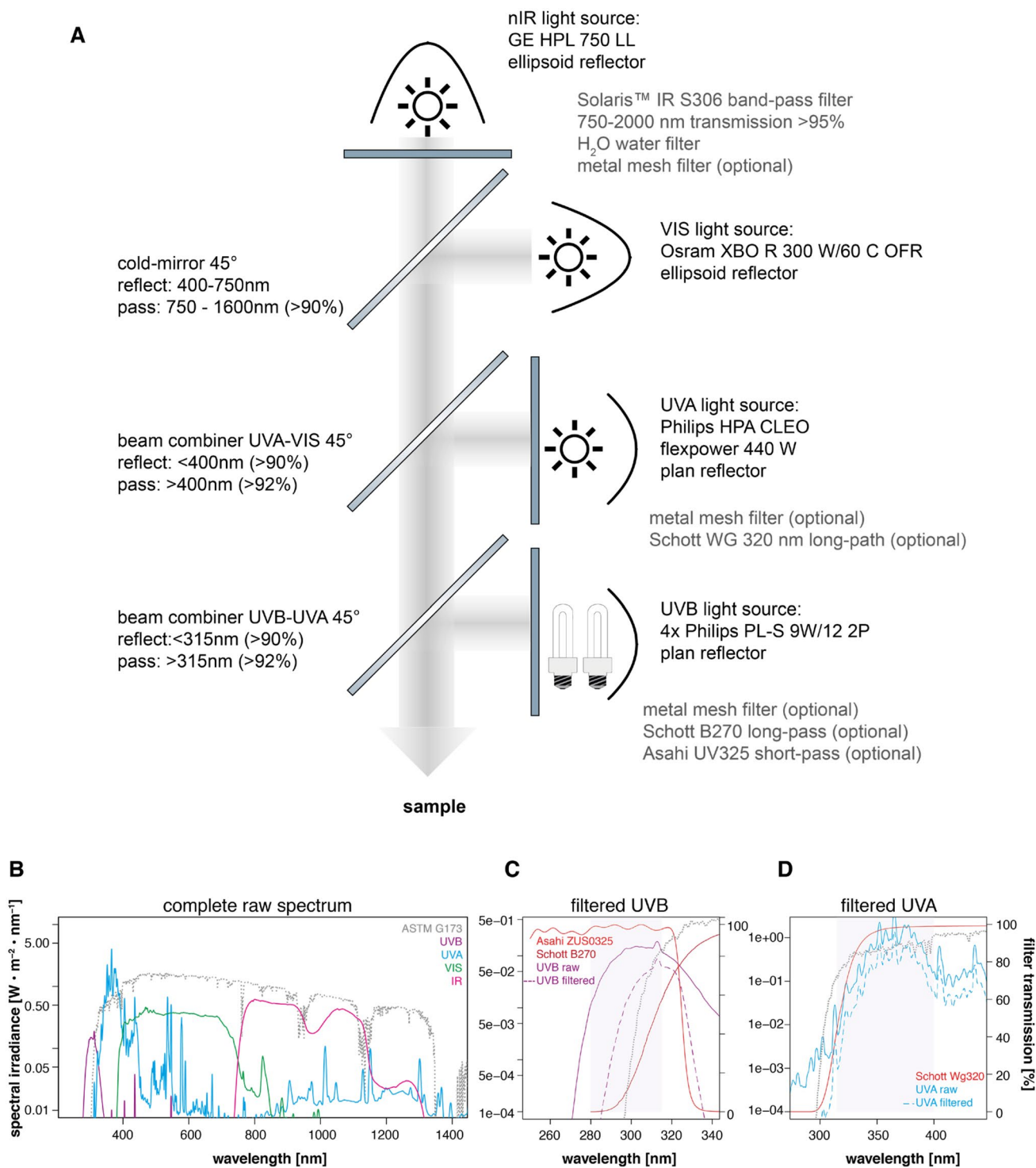
Fig. 1 **A** Schematic set-up of the irradiation device depicting the placement of the four lamps as well as the beam combiners and (optional) filters for the individual lamps. **B** Raw spectrum of the four individual lamps in relation to the ASTM G173 reference spectrum without additional optical or density filters, except for the IR spectrum, which is already filtered by the 2 cm water cuvette and the Solaris IR S306 filter. Y-axis in log scale. **C** and **D** Further filtering with long- and short-pass filters of the UVB and UVA lamps ensure the minimal spectral cross-contamination from one lamp to the other spectral bands. Additionally, the UVB tubes were filtered to ensure there is no detectable light below 280 nm, due to the high biological activity and unphysiological occurrence of these wavelengths. The shaded areas indicate the targeted spectral ranges for the indicated lamp

The emitted light from the four lamps was combined by three beam combiners (dichroic mirrors). First, a custom-made 315 nm (45°) beam combiner (S1 Optics, Germany) added the emission of the UVB lamps to the total spectrum. Second, a custom-designed 400 nm (45°) beam combiner (S1 Optics, Germany) was installed to add the UVA range. Third, a 750 nm (45°) cold mirror (Knight Optical) was used for the addition of the visible spectrum. The beam combiners dictated the positioning of the lamps. Since only short wavelength light can be reflected and long wavelength light passes through the dichroic mirrors, the UVB source had to be positioned closest to the sample area, whilst the infrared emitting lamp needed to be positioned with the greatest distance. The HPL 750 W LL lamp, used for the infrared part of the combined spectrum, was filtered by a 2 cm cooled water cuvette and a 750 nm long-pass filter (Solaris IR S306, PSC, Denmark). After the first assembly, we measured the spectral irradiance of the individual lamps as well as the combined irradiation (Fig. 1B) using a Spectro320-166 (Instrument Systems, Germany) spectrometer calibrated against a BN 9101 reference lamp (Gigahertz-Optik, Germany) in the range of 250–2800 nm. Based on these results, further modifications were implemented: the UVA lamp was filtered by a long-pass Schott WG 320 filter to prevent cross-contamination of the UVB spectrum with small amounts of UVB emitted from the UVA lamp. The UVB lamp was filtered with an Asahi Spectra UV325 short-pass filter (ZUS0325, Mountain Photonics, Germany). This filter blocked the emission of UVA from the UVB lamps. Additionally, a UVB long-pass filter (Schott B270, Reichmann Feinoptik, Germany) was used to filter out any UVC radiation. With this set-up, the spectral emissions of the UVA and UVB lamps were largely restricted to the targeted spectral bands (Fig. 1C and D, as well as Table 1). One exception was the emission of visible

light by both the UVA and UVB lamp. When compared to the normal environmental irradiance, however, the absolute values of visible light in this setting were still low (24% of ASTM G173).

Further adjustments refer to incorporating metal mesh filters with defined open apertures in front of the UVA and UVB lamps to achieve the desired ratio of UVA to UVB as well as irradiance similar to the ASTM G173 reference spectrum [31]. With these modifications, the resulting irradiance for the UVB and UVA spectral range was measured to be 0.64 ± 0.05 W/m^2 (UVB) and 41.6 ± 0.86 W/m^2 (UVA), respectively, corresponding to 94% and 91% of the ASTM G173 reference spectrum and a UVA to UVB ratio of 1:64 (close to the calculated ratio of 1:66 in the ASTM G173 reference spectrum). As mentioned above, the visible spectral range (400–750 nm) is under-represented and only reaches approximately 24% of integrated irradiance of the ASTM G173 reference spectrum (see above), whilst the near-infrared range had an irradiance of approximately 62% of the reference spectrum. All details are listed in Table 2.

To prevent nIR-related overheating, we integrated an actively cooled water filter, which efficiently reduces the thermal effects of IR irradiation. An external laboratory chiller pumps precooled water (11 °C) through the 2 cm infrared filter cuvette. The same chiller was used to cool Peltier elements, which in turn control the temperature of the irradiation chamber base plate (copper).

3.2 Physical validation of the irradiation devices

After final assembly of four identical irradiation devices, we performed several irradiation tests for the reproducibility and stability of the lamps. First, we analysed the homogeneity of the irradiated area (17 cm × 17 cm) by placing

Table 1 Spectral cross-contamination after additional filtering of the UVA and UVB lamps

	UVB band (280–315 nm)	UVA band (316–400 nm)	Vis band (401–750 nm)	IR band (751–1400 nm)
UVB lamp	100 ± 0	68 ± 6.27	132.93 ± 13.07	22.87 ± 7.41
UVA lamp	0.01 ± 0.01	100 ± 0	68.04 ± 6.92	11.53 ± 2.9
VIS lamp	0 ± 0	1.34 ± 0.38	100 ± 0	9.04 ± 1.13
IR lamp	0 ± 0	0 ± 0	0.29 ± 0.19	100 ± 0

The measured irradiance of each spectral band in four identically built devices was averaged and normalised to the irradiance in the targeted spectral band (100%, indicated in the column headers). Errors indicate the standard deviation. The numbers represent the percentage irradiance emitted in each band normalised to the irradiance in the targeted spectral band

Table 2 Irradiance in four spectral bands (percentage of ASTM G173 reference in brackets)

|	UVB (280–315 nm)	UVA (316–400 nm)	Vis (401–750 nm)	IR (751–1400 nm)
Irradiance [W m^{-2}]	0.64 ± 0.05 (94%)	41.6 ± 0.86 (91%)	119 ± 12.4 (24%)	218 ± 12.2 (62%)

Values present the average of four identically built devices and errors represent the standard deviation (compare to Figure S1C)

the measurement head of a calibrated portable spectrometer (Jeti specbos 1211UV, JETI Technische Instrumente, Germany) at 16 sites regularly spaced across the irradiation sample area (4 cm distance each in x and y directions) and measured the individual and total spectral emission (in the range of 250–1200 nm) of the irradiation devices. The irradiance variations between the different locations were found to be < 10%, except for three positions at the border, which showed variations of 11 and 12%, respectively (Figure S1A). These measurements were taken at the extreme edges of the sample area, locations that are rarely used in the experiments described in this study. Next, we assessed the temporal stability of the four irradiation devices by measuring the same position (central on the sample area) repeatedly (6 × over a time period of 1 h). The variations in the total integrated irradiance (270–1000 nm) were found to be < 10% in all four built devices, demonstrating stable irradiation conditions (Fig. S1B).

The average spectra of all four lamps were measured in the range from 250 to 1000 nm (Jeti specbos) at the same 16 positions in the sample area. Figure S1C shows the comparison of the four irradiation devices, indicating the reproducibility of the set-up and the spectral similarities. The largest variations were found in the visible spectral range (400–750 nm) with a coefficient of variation of 0.236 in contrast to the lower values found for the other spectral ranges: 0.065 (UVB), 0.057 (UVA) and 0.039 (nIR) respectively (see also Figure S1A). For a more biological relevant comparison, we performed a weighting of the raw spectral data with the CIE erythema action spectrum [32] (Fig. S1D). The integrated CIE-weighted UVB irradiance of the developed device was measured to be 0.177 W/m² and therefore higher than the ASTM G173 (0.051 W/m²) due to the cut-off of the ASTM G173 at 290 nm. This cut-off varies in natural conditions and is higher in the ASTM G173 spectrum [33]. In contrast, the integrated CIE-weighted irradiance in the UVA range was identical (0.039 versus 0.034 W/m²), for the AMST G173 spectrum and our device, respectively.

3.3 Comparability and consistency of four versions of the irradiation devices: biological validation of the radiation efficacy

In a ring trial, the CPD induction by the four build devices was measured after immuno-staining in a flow cytometer. The dose-dependent formation of CPDs is shown in Fig. 2 for each device individually with the indicated lamps activated and demonstrates that there were no significant differences between the four dose–response curves (one-way ANOVA with Bonferroni's post hoc test). In addition, we measured the CPD generation after exposure to UVA. We detected UVA-induced CPDs after identical exposure times required for 288 J/m² UVB corresponding to 22 kJ/m² UVA.
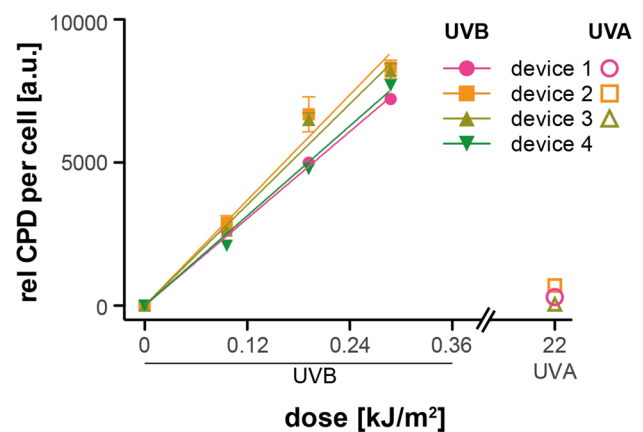
Fig. 2 Induction of CPDs by the four identically built irradiation devices. Shown are the relative intensity levels per cell detected by flow cytometry, after UVB exposure with the indicated doses and immune-fluorescence detection of CPDs. Plotted are the mean values of at least three biological replicates after subtraction of the fluorescence intensities of the control cells together with the standard error of the mean. Dose–response curves were linearly fitted. On the right, the levels of CPDs after UVA exposure are plotted

This exposure resulted in significantly higher CPD levels compared to controls, but approximately tenfold lower levels compared to 288 J/m² UVB. Considering the different radiant exposure values (doses), the CPD induction rate was ∼ 750-fold lower for the UVA exposure compared to the UVB exposure, and close to values reported earlier [34, 35].

3.4 Cellular metabolic activity as measured by MTT

HaCaT cells were exposed to single spectral bands as well as combinations thereof. The 0.36 kJ/m² UVB exposure corresponds according to [32] to an exposure of 4.6 min in mid-summer or approximately 53 min in winter (using Lauder, New Zealand as a reference measurement station (45°S, 170°E, altitude 370 m)). For the UVA range, the corresponding exposure times would represent 6.6 min in summer and 22 min in winter.

UVB exposure resulted in a significant dose- and time-dependent decrease in metabolic activity (based on the linear regression of the dose vs. the half-life time constant), detectable 24 h post irradiation (Figs. 3A and S3A). This decrease was on-going up to 72 h. The decrease in metabolic activity following all exposures was directly dependent on the dose and could therefore be fitted with a linear regression (Figure S3). For UVA exposure, we found a time-dependent, non-significant decrease in metabolic activity. This was only observed at doses above 82.5 kJ/m². Visible and nIR exposure did not result in a significant reduction of metabolic activity (Figs. 3C, D and S3C, D).

When UVB and nIR irradiation was applied simultaneously, the significant reduction in metabolic activity was
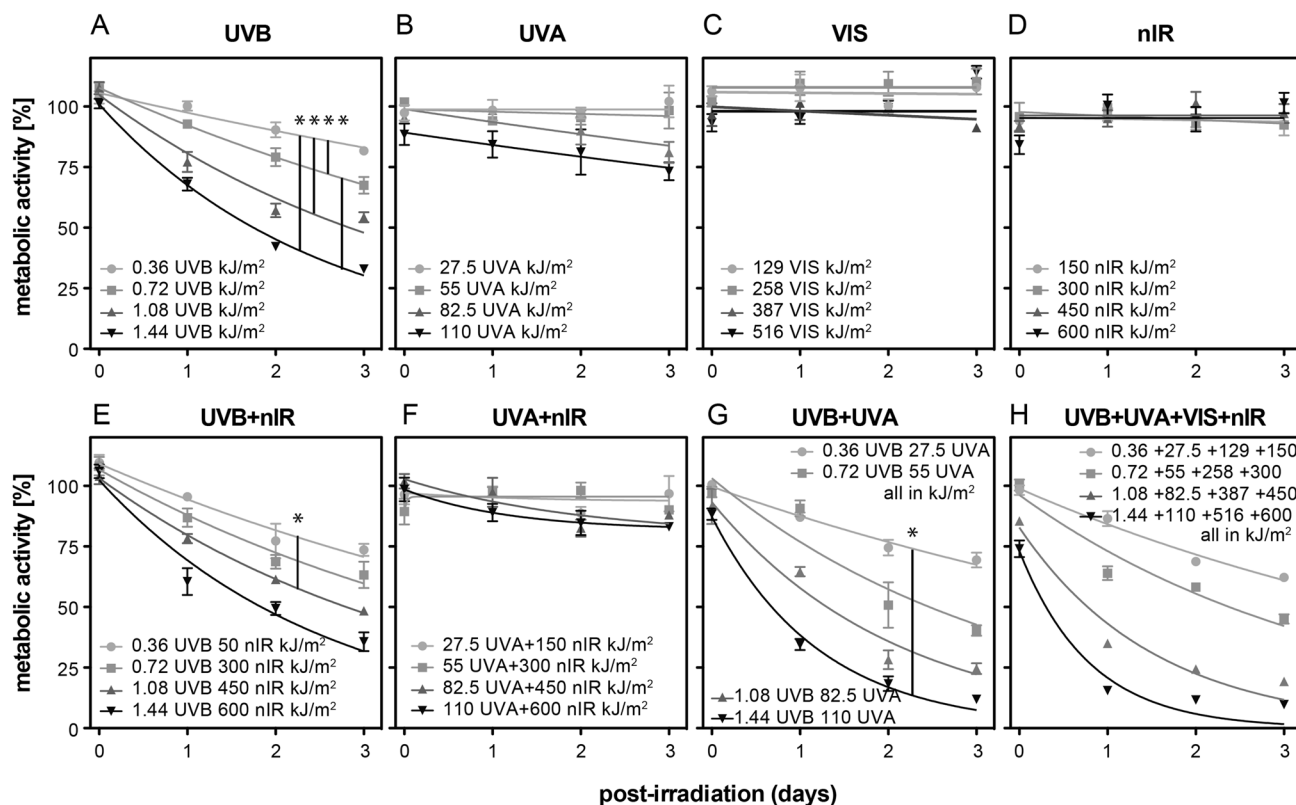
Fig. 3 Metabolic cellular activity was assessed using the MTT assay directly after irradiation (day 0) and 24 h, 48 h, and 72 h post irradiation for individual spectral bands UVB (**A**), UVA (**B**), VIS (**C**) and nIR (**D**). Additionally combinations of spectral bands were analysed: UVB+nIR (**E**), UVA+nIR (**F**), UVB+UVA (**G**) as well as the complete spectrum (**H**). Each condition/dose was at least measured in three biological replicates with two technical replicates each and normalised to the corresponding sham-irradiated control. The plotted values represent the means of the replicates together with the stand-ard error of mean. Doses are represented in different grey levels and the resulting data points were fitted using a one-phase decay function. Statistical significance of the different decay curves was estimated based on the half-life fitting parameter and its corresponding 95% confidence interval (CI). In cases where the CI did not overlap (pair-wise analysis), the one-phase decay curves were assigned significant difference (*) based on a *p* value of 0.05. The dose-dependent curves for each day are shown in Figure S3

similar to the reduction observed for cells exposed to UVB only (Fig. 3E and S3E). Simultaneous exposure to UVA and nIR did not show a significant effect at lower doses (27.5 kJ/m^2 UVA + 150 kJ/m^2 nIR and 55 + 300 kJ/m^2 nIR) and led to a non-significant reduction in metabolic activity at higher doses, mainly at day 2 and 3 (Figs. 3F and S3F). In contrast, when UVA and UVB were applied simultaneously, metabolic activity decreased significantly stronger (smaller half-life time) than for individually applied UVA or UVB (up to 1.5-fold). The dose-dependent decrease in metabolic activity occurred directly after irradiation and the trend was persistent, although not significant, at day 1 and 2 after exposure to simultaneous UVA and UVB radiation (Figs. 3H and S3H).

Irradiation with the full spectrum caused the same toxic profile as the combination of UVA and UVB, demonstrating that VIS and nIR did not modulate the cells' metabolic activity when combined with UVA and UVB. The main difference between UVA + UVB exposure compared to the complete spectrum is the metabolic activity seen at the first and

second time point. There, the complete spectrum reduced the metabolic activity even stronger (not significant) than in the UVA + UVB exposed cells, although VIS and nIR alone do not show any negative effect on cell metabolism (Fig. 3H).

3.5 Cell cycle modulation of combined spectral bands

Next, we asked whether the different irradiation regimes would affect the cell cycle of the surviving cells. UVB exposure led to the most pronounced biological response. As an early effect 2 h post irradiation—UVB induced a significant G$_1$ arrest followed by a significant S-phase increase 12–16 h after exposure (Fig. 4A) as also reported in [36]. After that, a significant increased G$_2$/M fraction was detected (18 h). Then the cell cycle distribution started to return back to normal levels. UVA exposure with 27.5 kJ/m^2 showed less-pronounced cell cycle alterations with as significant increase in S-phase cells directly after exposure up to 2 h post exposure
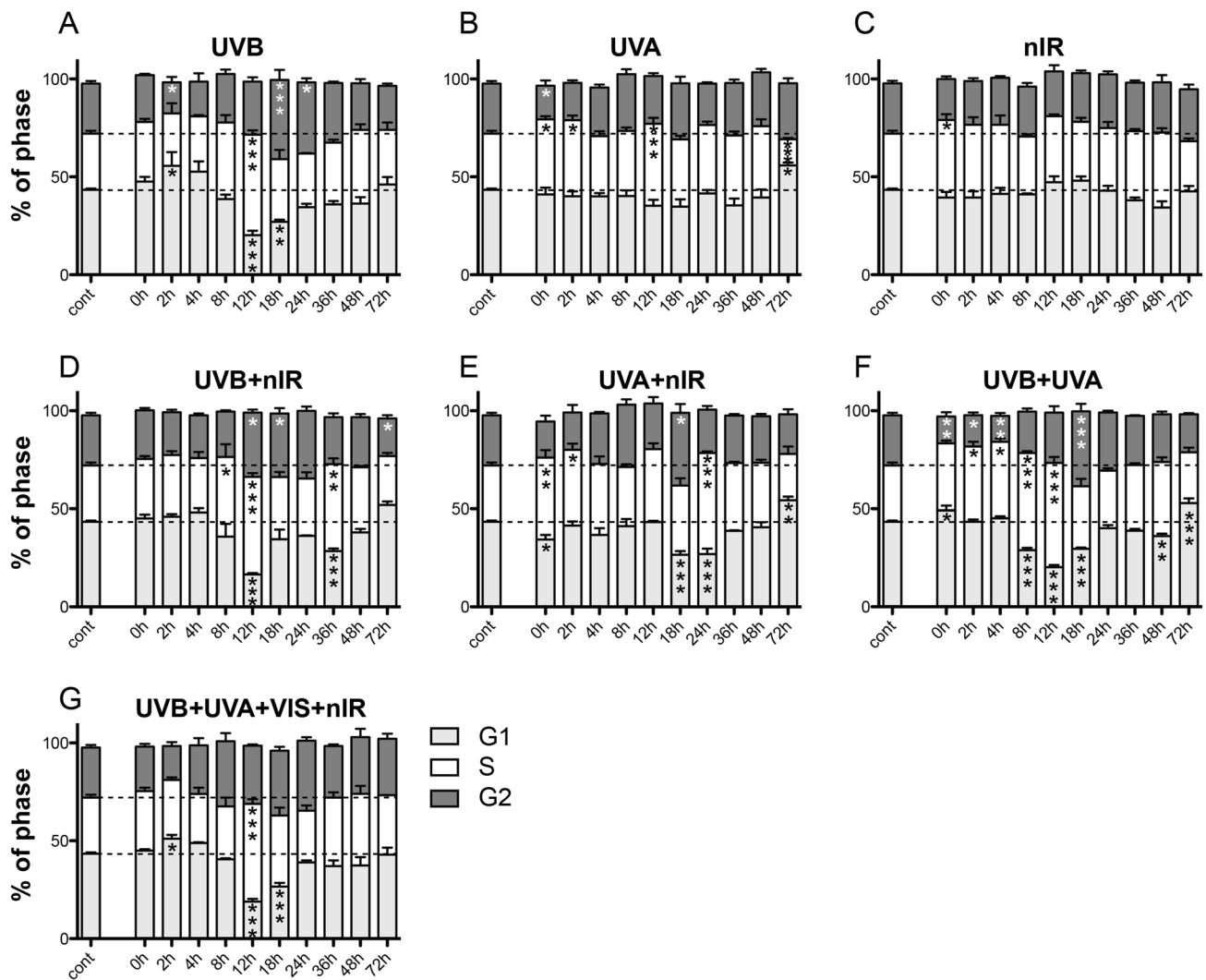
Fig. 4 Cell cycle distribution of HaCaT cells after exposure to individual spectral components (**A**–**C**) and combinations thereof (**D**–**G**). Cells were harvested at the indicated times and analysed using flow cytometry. The cell cycle distributions were calculated based on the quantification of the DNA content after propidium iodide staining and then fitted, using the Dean–Jett–Fox algorithm (FlowJo). An example workflow, including the gating steps is shown in Figure S4. The bars represent the average percentage of cells assigned to the corresponding cell cycle phases and are based on at least 4 biological replicates per dose and condition. The error bars represent the standard error of the mean. The cell cycle distribution of control cells is shown at the left of each subplot and the G_1, S and G_2 fractions are shown as dotted lines. Significance was tested against the control for G_1, S and G_2 populations individually. $*p \leq 0.05$; $**p \leq 0.01$; $***p \leq 0.001$

(Fig. 4B). A significant increase in S-phase cells was found 12 h and a significant reduction of S-phase cells at 72 h post exposure. After nIR irradiation, we only observed a significant increase of S-phase cells directly after exposure. All other tested time points did not show significant changes in the cell cycle distribution (Fig. 4C).

When UVB was simultaneously applied with nIR, the significant S-phase arrest at 12 h post irradiation was found similar to the arrest seen with UVB alone (Fig. 4A and D). Interestingly, the initial G_1 arrest (2–4 h post irradiation) was not detectable in the co-exposed cells (UVB + nIR) and the subsequent release was faster in UVB + nIR exposed cells compared to UVB exposed

cells alone. UVB and UVA co-exposed cells showed the most pronounced cell cycle alterations with an extended significant S-phase arrest already 8 h post irradiation and lasting until 12 h. This exposure condition also induced the early G_1 arrest (directly after exposure). The late G_1 arrest (72 h) was commonly found (Fig. 4B, E and F) in UVA, UVA + nIR and UVA + UVB exposed cells. When UVA was combined with nIR, we found a smaller, but significant S-phase arrest 18–24 h post irradiation. This arrest was stronger when compared to the individual irradiations or the additive effect thereof (Fig. 4B and E). Most notably, when the full spectrum (UVB + UVA + VIS + nIR) was applied, the cell cycle distribution resembles that of

UVB only, with the S-phase arrest at 12 h post exposure as the predominant effect (Fig. 4G) and no significant late G_1 arrest.

Taken together, we can conclude that the cell cycle is significantly affected by UVB exposure (0.36 kJ/m^2). Co-exposure with UVA (27.5 kJ/m^2) or nIR (150 kJ/m^2) exerts some modulation; however, as part of the entire solar spectrum, these effects do not seem to become effective.

3.6 Clonogenic survival of UVB exposure is modulated by co-exposure with both UVA and nIR

Finally, we asked whether and how the above-identified early effects would impact on the long-term growth capacity of the HaCaT cells. To address this, we performed clonogenic survival (or colony forming) assays. First, we produced dose-dependent survival curves for the individual spectral bands (UVA, UVB and nIR). Whilst UVB exposure (120–720 J/m^2) resulted in a significant
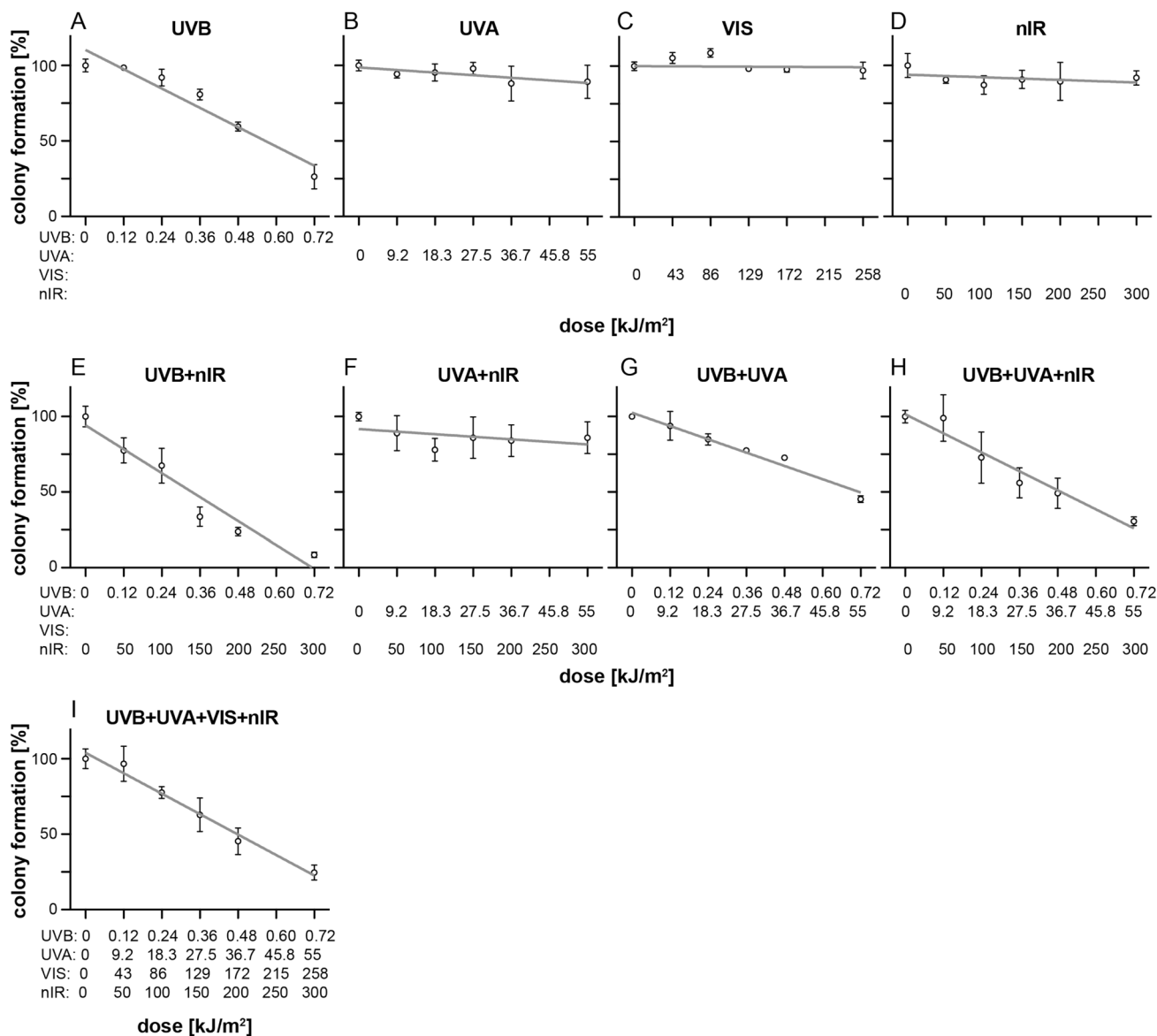
Fig. 5 Clonogenic survival obtained from irradiated HaCaT cells. Depicted are the colony formation results for individual spectral bands (**A–D**) as well as for irradiation with combined spectral bands (**E–I**). The impact of each irradiation treatment was measured at least in three biological replicates and normalised to the corresponding sham-irradiated control. The plotted values represent the means of the replicates, together with the standard error of mean. The doses for each individual or combined exposure are given at the x-axis. Linear curves were fitted (grey lines). Examples of the colonies are shown in Figure S3. Statistical testing whether the fitted linear slopes are significantly different from zero revealed significance for **A**, **E**, **G**, **H** and **I**

linear dose-dependent reduction in colony number with $-10.66 \pm 1.48\%$ per 100 J/m^2, UVA (9.2–55 kJ/m^2), VIS (0–258 kJ/m^2) and nIR exposure (0–300 kJ/m^2) did not cause significant linear relationship between dose and reduction in colony formation ($-18.73 \pm 7.4\%$ per 100 kJ/m^2, $-2.75 \pm 2.14\%$ per 100 kJ/m^2 and $-1.7 \pm 1.8\%$ per 100 kJ/m^2 respectively) (Fig. 5 A-D). When UVB was combined with nIR, the cytotoxic effect was significantly increased as compared to UVB irradiation alone (Fig. 5E vs. 5A and S5). The dose-dependent reduction in colony formation increased from $-10.66 \pm 1.48\%$ to $-13.22 \pm 1.65\%$ per 100 J/m^2. This additive cytotoxic effect was not seen upon simultaneous irradiation of UVA and nIR (Fig. 5B vs. F), where the dose–effect curves had similar slopes (-18.73 and -18.53% per 100 kJ/m^2). Interestingly, when UVA was simultaneously applied with UVB, the cytotoxic effect of UVB was mildly, but significantly reduced (Fig. 5A vs. B vs. G) from -10.66 to -7.35% per 100 J/m^2. When we combined three or all four spectral bands, we found a cytotoxic effect similar to that of UVB alone (Fig. 5A vs. H).

3.7 Proliferative expansion (colony size) is influenced by UVB

As an additional parameter for the radiation effect on long-term cell survival, we analysed the resulting colony sizes in the clonogenic survival assay. Whilst nIR exposure did not modulate growth of the HaCaT cells, UVA decreased the colony size significant for doses of 27.5 and 36.7 kJ/m^2. UVB caused a significant increase in colony size with low-dose radiation 0.12 kJ/m^2 (Fig. 6) and a dose-dependent decrease at higher doses (0.48 and 0.72 kJ/m^2).

When UVA and UVB irradiation was combined, a significant decrease in colony size was seen for all doses. Accordingly, most prominent changes in colony size distribution were only seen upon radiation with combinations including UVB. With UVA + B as well as UVB + nIR, the primary increase in colony size was lost, compared to UVB exposure alone and the overall decrease in colony size was attenuated, demonstrating a modulatory effect upon combination. As part of the entire spectrum, however, the UVB effect was dominant with an increase at the lowest dose and decline of the colony size thereafter, although these observations are not significant due to the large size variations of the individual measurements. Again, this demonstrates that in combination, the individual wavelengths act differently, i.e. do not exert a defined action spectrum but rather the combination of wavelengths determines their individual contribution in modulating cellular events.

4 Discussion

Solar radiation and in particular solar UV radiation is of outmost importance, not least, because of its contribution to skin ageing and skin cancer. Accordingly, there is a longstanding interest in the role of UVB and UVA [1, 37]. More recently, also IR and VIS gained interest and were investigated more extensively concerning their contribution to cellular damage [24, 38–41]. However, the effect of the solar spectrum (ss) with all its wavelength combinations, is not well understood and is likely far more complex than the combined (additive) action of all individual wavelengths. Consequently, questions have arisen about the combined exposure to UVR (UVB and UVA) IR, and VIS and their intracellular action spectrum, i.e. whether additive/synergistic or even modulatory/antagonistic interactions occur.

Concerning the biological action spectrum, it was shown that all four wavelengths (UVB, UVA, VIS, and IR) induce ROS in skin cells (Zastrow et al. [18] and references therein) and besides inducing different rates of ROS, the different wavelengths may do so through non-overlapping mechanisms. To become effective however, the ROS level has to exceed the physiological range in a certain time period. Therefore, it is further suggested that all spectral bands may act in an additive/synergistic way when being applied to skin cells simultaneously, i.e. through the solar spectrum. However, a clear interactive role is still elusive.

All this demonstrates that the comparison of single and combined radiation qualities (different wavelength combinations) is essential and requires further investigation. The studies, however, also indicate that the technical requirements for respective studies are still insufficient. Frequently, irradiation devices only allow for a restricted set of simultaneous combinations [42–44], or combinatorial irradiation is performed sequentially [45, 46].

We, therefore, conceived and constructed a radiation device that enables irradiation across the entire UVB, UVA, VIS, and nIR range and can also generate the individual wavelength bands as well as any combination therefrom. Importantly, whilst combinations have frequently been applied sequentially [47, 48], our radiation device is constructed for simultaneous irradiation of all possible combinations. Furthermore, this device has proven to be stable for the irradiation of conventional cultures as well as 3D organotypic cultures for both acute and chronic exposure. As an example, 3D skin equivalents were irradiated 3 times a week for as long as 10 weeks without changes in the radiation quality (Boukamp, Pavez Lorie personal communication and [49]), thus making the presented irradiation device unique and demonstrating its broad scope of application.

We here utilised this device to demonstrate biological effects following acute irradiation of HaCaT cells with
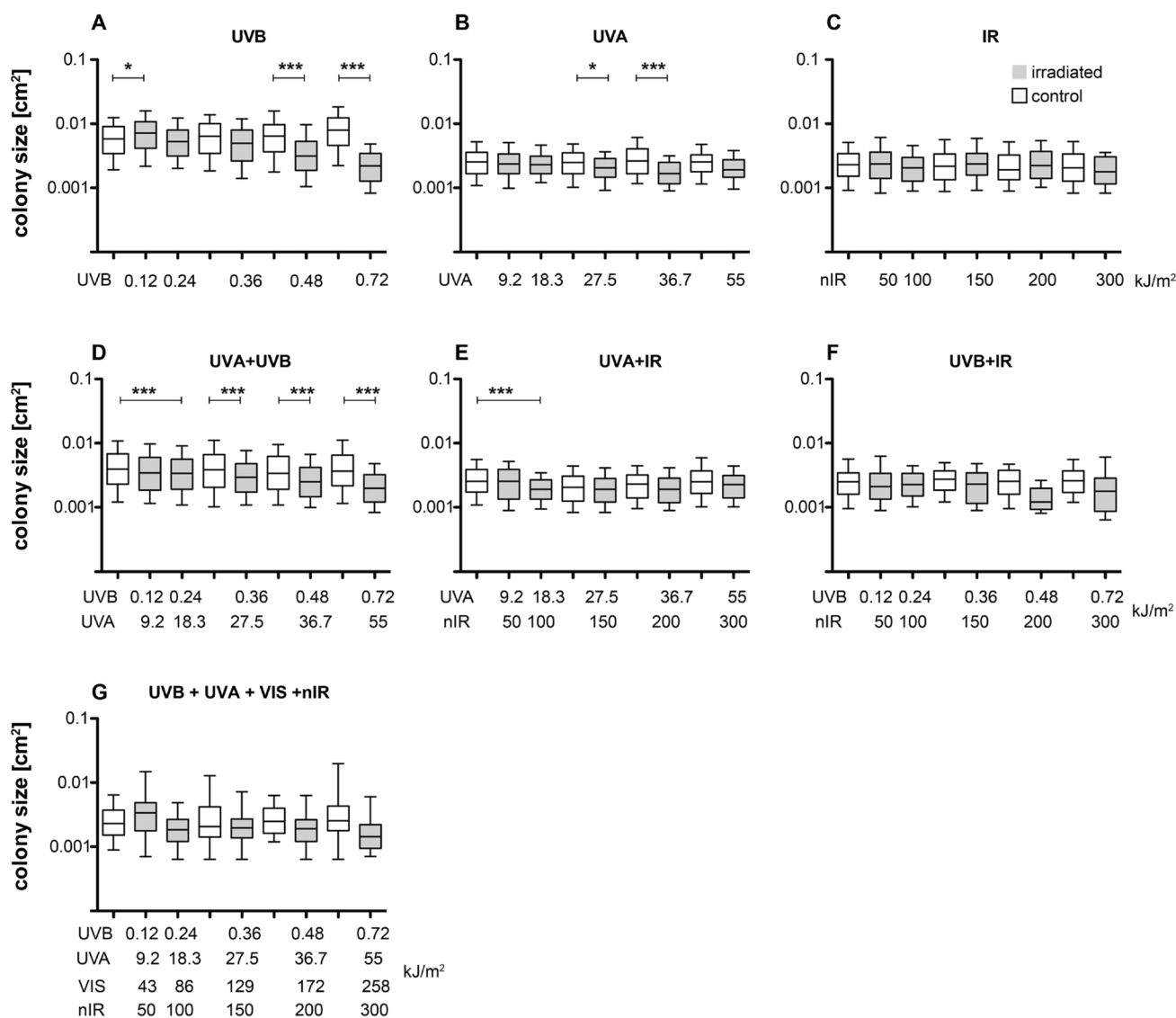
Fig. 6 Colony sizes in the clonogenic survival assay after irradiation with individual and combinations of spectral bands. **A–C** Individual spectral band exposures by UVB, UVA and nIR respectively. **D–F** Combinations of two spectral bands as indicated. **G** Full spectrum irradiation. Displayed are the size distributions of the colonies obtained after exposure (grey boxes) together with the sham-irradiated controls (white boxes). The first control represents the unirradiated control that was kept in PBS for the same duration as the second irradiation dose (approximately 5 min) and was used as reference control for the first two exposures. Longer exposures were normalised to the time-matched sham-irradiated control. Each bar is the result of the pooled colonies obtained from at least 3 biological replicates. Boxes represent the 25th to 75th percentile and whiskers extend to the minimum and maximum. The solid line represents the median. Significance was tested for each group vs its corresponding control using one-way ANOVA test with Bonferroni post test using a significance level of 0.05. $*p \leq 0.05$; $**p \leq 0.01$; $***p \leq 0.001$

all four individual spectral bands as well as all possible combinations thereof, including the solar UV spectrum (simultaneous UVB and UVA irradiation) as well as the entire spectrum (simultaneous irradiation with UVB + UVA + VIS + nIR). With this, we aimed to address the question of whether and how the different wavelengths would influence each other, respectively whether synergistic/additive or modulatory effects are seen with respect to different biological endpoints.

As proof-of-principle, we investigated three basic biological principles, namely sensitivity towards radiation (toxicity measured by MTT test) and cell cycle regulation, as well as long-term growth (colony formation) upon radiation with the different wavelengths and combinations.

So far, more complex comparative studies are rare. One corresponding work was recently performed utilising the Newport solar simulator and IR/VIS blocking filters to allow for irradiation with the entire solar spectrum versus the

solar UV spectrum [24]. In this publication, Birch-Machin and coworkers investigated primary human keratinocytes and fibroblasts exposed to individual and combined irradiation of the IR, VIS, and UV. ROS induction as well as mitochondrial and nuclear damage were studied [24]. They found a greater induction of these three endpoints with the solar spectrum radiation as compared to solar UV radiation alone (sUV). Interestingly, they even found a clear difference between epidermal keratinocytes and dermal fibroblasts, thereby demonstrating differences in response to different wavelengths combinations as well as differences in the response pattern of the two skin cell types, with fibroblasts being more affected than keratinocytes.

Concerning our studies, measuring sensitivity to radiation by means of cellular metabolic activity (MTT test) was already informative. Whilst UVB showed significant dose-dependent toxicity, UVA exhibited an only minor toxic effect at higher doses. VIS and nIR did not confer toxicity. These findings are in line with previous reports showing that VIS (36 J/cm^2) is non-toxic for HaCaT cells. Cytotoxic effects of VIS exposure are dependent on the presence of melanin, which is not found in HaCaT cells [40, 50], but other sensitizers might be involved as well, such as β-carotene, porphyrins or flavins [51]. With respect to the isolated nIR exposure, we did not find enhanced cell survival/metabolic activity as reported for high irradiance laser exposure of L929 mouse fibroblasts [52]. This might be due to the different cell type used (fibroblasts *versus* epithelial cells), the power levels, and/or a specific wavelength effect. Accordingly, nIR-addition did not alter the toxicity profile when combined with UVB or UVA. However, simultaneous radiation with UVB and UVA either as sUV radiation or in combination with VIS and IR radiation, showed synergism, leading to clearly increased toxicity. Observed impairment of metabolic competence in irradiated cells may have resulted from oxidative stress, which is a self-propagating process. Therefore, initial oxidative damage, resulting from radiation-excited state of the cellular components or by photosensitization, creates additional free radicals that damage mitochondria and consequently leads to further ROS production [53]. It was demonstrated for excised human skin that not only UVA and UVB radiations were responsible for the radical production during sun exposure, but also that up to 50% of the radicals were produced by the VIS/nIR radiation. Therefore, the synergetic effect of the entire spectrum may result from activation of several ROS promoting pathways, with different chromophores and cell components being involved in free radical production elicited by solar spectrum wavelengths that finally enhance and promote each other (Fig. 3H).

Regarding cell cycle regulation, in vitro studies have shown that UVB irradiation is capable of inducing a cell cycle arrest in G$_1$ phase, thereby delaying S-phase [54, 55].

We find an early UVB-dependent G$_1$ arrest (after 2–4 h) whilst this is missing upon UVA radiation. It was recently suggested that "a less-effective cell cycle arrest with UVA may render UVA-induced pyrimidine dimers more mutagenic than UVB-induced ones" [56]. As part of the solar spectrum, the role of UVA in cell cycle regulation may, however, be less clear. Our data suggest that within the entire solar spectrum, UVB is the foremost in cell cycle regulation whilst UVA does not seem to contribute excessively. In agreement with reports by others [56], we found UVA-related cell cycle effects at significantly higher doses, i.e. starting from 100 kJ/m^2 (data not shown). This in turn indicates that in combination, the action profile of the individual wavelength is subject to modification and that for a realistic (human) risk assessment, the entire solar spectrum will prove to be the gold standard.

It needs to be appreciated that the G$_1$ arrest is predominated by p53 and may not be as extensive in HaCaT cells that carry p53 mutations in both alleles of the p53 gene [57]. However, this detailed study demonstrates that UVB and to some extent also the entire solar spectrum is able to induce an early G$_1$ arrest also in the HaCaT cells, supporting a role for a p53-independent mechanism in inducing a G$_1$-to S-phase delay in p53-deficient keratinocytes [58]. These findings are in agreement with earlier reported cell cycle perturbation following UVB, considering the p53 status of the HaCaT cells [56, 59–61]. Of note, the UVB-dependent arrest seems to be suppressed when combined with UVA or nIR exposure but not when being part of the entire solar spectrum, demonstrating the importance of differential interactive regulations.

Twelve hours after UVB radiation, the cells experience a strong S-phase boost. Accumulation of S-phase cells was also described earlier, and in vivo studies support evidence for a mitogenic response of UVB irradiation [62]. In hairless mice (hr/hr), an increase in S-phase was observed as early as 12 h after treatment with a sub-erythema dose of 12.5 mJ per cm^2 or an erythema dose of 25 mJ per cm^2 [63, 64]. In line with this interpretation, UVB alone as well as all combinations containing low-dose UVB (0.36 kJ/m^2) favoured the development of large colonies indicative of an enhanced proliferation rate as also reported in [65].

Whilst nIR did not exhibit any obvious cell cycle regulation, UVA provoked a late (72 h) G$_1$ arrest. Whereas dominant also in different combinations, this UVA-dependent G$_1$ arrest was no longer effective when UVA was part of the entire solar spectrum demonstrating the more complex modulation when all wavelengths were combined.

To investigate for more long-term effects, we additionally assayed for colony formation following the different radiation regimes. Again, the dominant dose-dependent toxicity of UVB was reflected in the cells' ability to generate colonies. Our results for UVA and UVB reduced colony

formation is in line with previously reported values, e.g. [66]. The UVB-related cytotoxicity also dominated any combination with other spectral components. Interestingly, the combination of UVB and nIR caused an even stronger dose-dependent decrease in the number of colonies, whilst in combination with UVA, the effect was reduced. Since the molecular mechanism underlying these phenotypes are still elusive, these findings once more demonstrate that, although on their own not affecting the investigated growth parameters, in combination they can be of the modulatory effects for the cells. It is well known that the different wavelengths are absorbed by different chromophores; therefore, the final action spectrum is not a simple addition of the individual action spectra but an interplay of all four action spectra.

Whilst the MTT test is a measure for toxicity, i.e. immediate cell death, the clonogenic or colony formation assay adds in determining the ability of single cells to expand into colonies, thereby test the cell's regenerative capacity and with that the ability to maintain or even improve their proliferative potential. Accordingly, many studies performed with this assay have established extensive information on the sensitivity to, e.g. radiation or chemotherapeutics but also about recovering from such insults (number and size of the colonies). We now add, using this new radiation source, that UVB alone and in all combinations (UVA, nIR and VIS) is the most toxic wavelength (MTT test, colony number). It is, however, noteworthy that the colony size seems to increase upon low-dose UVB radiation either alone or as part of the entire solar spectrum. With higher doses and in a dose-dependent manner, a decline in colony size is induced. This fact points to a differential response and importantly applies for the entire solar spectrum, and may be of relevance for the radiation response in humans. Therefore, this low-dose UV effect will be further investigated.

In conclusion, we here present a radiation device that besides the combined UVB, UVA, VIS and nIR (with an integrated irradiance distribution close to natural sunlight) allows for the irradiation with the individual spectra as well as any combination thereof. Thereby, it allows for the identification of additive synergistic or even modulatory effects provided by the individual wavelengths as well as their combinations thereof including that of the full spectrum (UVB to nIR) with the same device and thus with the same and directly comparable spectral distribution within the solar spectrum. Accordingly, we can show that cell death is predominantly determined by UVB, though augmented in combination with UVA. Also, the cell cycle is most significantly affected by UVB exposure. Co-exposure with UVA or nIR exerts some modulation, which is lost when being part of the entire solar spectrum. Clonogenic activity that is mostly affected by UVB extend is suppressed by UVA and increased by nIR co-exposure. In the entire spectrum, the UVA and nIR effects are neutralised.

Availability of data and material (data transparency) All primary data are available from the TU datalib (https://tudatalib.ulb.tu-darmstadt.de/handle/tudatalib/1126).

Code availability (software application or custom code) Not applicable.

Declarations

Conflict of interest The design of the irradiation device is covered by a patent application (10 2022 102 915.8) filed at the Deutsches Patent- und Markenamt (German Patent and Trade Mark Office) by the authors.

References

1. de Assis, L. V. M., Tonolli, P. N., Moraes, M. N., Baptista, M. S., & de Lauro Castrucci, A. M. (2021). How does the skin sense sun light? An integrative view of light sensing molecules. *Journal of Photochemistry and Photobiology C, 47*, 100403.
2. Pearse, A. D., Gaskell, S. A., & Marks, R. (1987). Epidermal changes in human skin following irradiation with either UVB or UVA. *The Journal of Investigative Dermatology, 88*(1), 83–87.
3. Wischermann, K., Popp, S., Moshir, S., Scharfetter-Kochanek, K., Wlaschek, M., de Gruijl, F., Hartschuh, W., Greinert, R., Volkmer,

B., Faust, A., Rapp, A., Schmezer, P., & Boukamp, P. (2008). UVA radiation causes DNA strand breaks, chromosomal aberrations and tumorigenic transformation in HaCaT skin keratinocytes. *Oncogene, 27*(31), 4269–4280.

4. Greinert, R., Detzler, E., & Harder, D. (2000). The kinetics of postirradiation chromatin restitution as revealed by chromosome aberrations detected by premature chromosome condensation and fluorescence in situ hybridization. *Radiation Research, 154*(1), 87–93.

5. Mitchell, D. L., Volkmer, B., Breitbart, E. W., Byrom, M., Lowery, M. G., & Greinert, R. (2001). Identification of a non-dividing subpopulation of mouse and human epidermal cells exhibiting high levels of persistent ultraviolet photodamage. *The Journal of Investigative Dermatology, 117*(3), 590–595.

6. Rapp, A., & Greulich, K. O. (2004). After double-strand break induction by UV-A, homologous recombination and nonhomologous end joining cooperate at the same DSB if both systems are available. *Journal of Cell Science, 117*(Pt 21), 4935–4945.

7. Yoon, J. H., Lee, C. S., O'Connor, T. R., Yasui, A., & Pfeifer, G. P. (2000). The DNA damage spectrum produced by simulated sunlight. *Journal of Molecular Biology, 299*(3), 681–693.

8. Arlett, C. F., Lowe, J. E., Harcourt, S. A., Waugh, A. P., Cole, J., Roza, L., Diffey, B. L., Mori, T., Nikaido, O., & Green, M. H. (1993). Hypersensitivity of human lymphocytes to UV-B and solar irradiation. *Cancer Research, 53*(3), 609–614.

9. Sayre, R. M., Cole, C., Billhimer, W., Stanfield, J., & Ley, R. D. (1990). Spectral comparison of solar simulators and sunlight. *Photodermatology, Photoimmunology and Photomedicine, 7*(4), 159–165.

10. Sayre, R. M., Stanfield, J., Bush, A. J., & Lott, D. L. (2001). Sunscreen standards tested with differently filtered solar simulators. *Photodermatology, Photoimmunology and Photomedicine, 17*(6), 278–283.

11. Marionnet, C., Tricaud, C., & Bernerd, F. (2014). Exposure to non-extreme solar UV daylight: Spectral characterization, effects on skin and photoprotection. *International Journal of Molecular Sciences, 16*(1), 68–90.

12. Colarossi, D., Tagliolini, E., Principi, P., & Fioretti, R. (2021). Design and validation of an adjustable large-scale solar simulator. *Applied Sciences, 11*(4), 1964.

13. Tawfik, M., Tonnellier, X., & Sansom, C. (2018). Light source selection for a solar simulator for thermal applications: A review. *Renewable and Sustainable Energy Reviews, 90*, 802–813.

14. López-Fraguas, E., Sánchez-Pena, J. M., & Vergaz, R. (2019). A Low-Cost LED-Based Solar Simulator. *IEEE Transactions on Instrumentation and Measurement, 68*, 4913–4923.

15. Kolberg, D., Schubert, F., Lontke, N., Zwigart, A., & Spinner, D. M. (2011). Development of tunable close match LED solar simulator with extended spectral range to UV and IR. *Energy Procedia, 8*, 100–105.

16. Godar, D., Miller, S., & Thomas, D. (1994). Immediate and delayed apoptotic cell death mechanisms: UVA versus UVB and UVC radiation. *Cell Death and Differentiation, 1*(1), 59–66.

17. De Gruijl, F. R. (2000). [33] Photocarcinogenesis: UVA vs UVB. *Methods in Enzymology, 319*, 359–366.

18. Zastrow, L., Groth, N., Klein, F., Kockott, D., Lademann, J., Renneberg, R., & Ferrero, L. (2009). The Missing Link – Light-Induced (280–1,600 nm) Free Radical Formation in Human Skin. *Skin Pharmacology and Physiology, 22*(1), 31–44.

19. Duteil, L., Cardot-Leccia, N., Queille-Roussel, C., Maubert, Y., Harmelin, Y., Boukari, F., Ambrosetti, D., Lacour, J.-P., & Passeron, T. (2014). Differences in visible light-induced pigmentation according to wavelengths: A clinical and histological study in comparison with UVB exposure. *Pigment Cell and Melanoma Research, 27*(5), 822–826.

20. Sondenheimer, K., & Krutmann, J. (2018). Novel means for photoprotection. *Frontiers in Medicine, 5*, 162.

21. Menezes, S., Coulomb, B., Lebreton, C., & Dubertret, L. (1998). Non-coherent near infrared radiation protects normal human dermal fibroblasts from solar ultraviolet toxicity. *Journal of Investigative Dermatology, 111*(4), 629–633.

22. Diffey, B., & Osterwalder, U. (2017). Labelled sunscreen SPFs may overestimate protection in natural sunlight. *Photochemical and Photobiological Sciences, 16*(10), 1519–1523.

23. Grandi, C., & D'ovidio, M. C. (2020). Balance between health risks and benefits for outdoor workers exposed to solar radiation: An overview on the role of near infrared radiation alone and in combination with other solar spectral bands. *International Journal of Environmental Research and Public Health, 17*(4), 38–39.

24. Hudson, L., Rashdan, E., Bonn, C. A., Chavan, B., Rawlings, D., & Birch-Machin, M. A. (2020). Individual and combined effects of the infrared, visible, and ultraviolet light components of solar radiation on damage biomarkers in human skin cells. *The FASEB Journal, 34*(3), 3874–3883.

25. Zastrow, L., & Lademann, J. (2016). Light-Instead of uv protection: New requirements for skin cancer prevention. *Anticancer Research, 36*(3), 1389–1394.

26. Sage, E., Lamolet, B., Brulay, E., Moustacchi, E., Chteauneuf, A., & Drobetsky, E. A. (1996). Mutagenic specificity of solar UV light in nucleotide excision repair-deficient rodent cells. *Proceedings of the National Academy of Sciences of the United States of America, 93*(1), 176–180.

27. Bustamante, M., Hernandez-Ferrer, C., Tewari, A., Sarria, Y., Harrison, G., Puigdecanet, E., Nonell, L., Kang, W., Friedländer, M., Estivill, X., González, J., Nieuwenhuijsen, M., & Young, A. (2020). Dose and time effects of solar-simulated ultraviolet radiation on the in vivo human skin transcriptome. *The British Journal of Dermatology, 182*(6), 1458–1468.

28. Cadet, J., & Wagner, J. (2013). DNA base damage by reactive oxygen species, oxidizing agents, and UV radiation. *Cold Spring Harbor Perspectives in Biology*. https://doi.org/10.1101/CSHPERSPECT.A012559

29. Boukamp, P., Petrussevska, R. T., Breitkreutz, D., Hornung, J., Markham, A., & Fusenig, N. E. (1988). Normal keratinization in a spontaneously immortalized aneuploid human keratinocyte cell line. *The Journal of Cell Biology, 106*(3), 761–771.

30. Riss, T. L., Moravec, R. A., Niles A. L., Duellman, S., Benink, H. A., Worzella, T. J. & Minor, L. (2013). Cell viability assays. In: Markossian, G. S., Sittampalam, A., Grossman, K., Brimacombe, M., Arkin, D., Auld, C. P., Austin, J., Baell, J. M. M., Caaveiro, T. D. Y., Chung, N. P., Coussens, J. L., Dahlin, V., Devanaryan, T. L., Foley, M., Glicksman, M. D., Hall, J. V, Haas, S. R. J., Hoare, J., Inglese, P. W., Iversen, S. D., Kahl, S. C., Kales, S., Kirshner, M., Lal-Nag, Z., Li, J., McGee, O., McManus, T., Riss P., Saradjian, O. J., Trask Jr., J. R., Weidner, M. J., Wildey, M., Xia & Xu, X. (eds). *Assay Guidance Manual*. Bethesda (MD): Eli Lilly & Company and the National Center for Advancing Translational Sciences (2004). Available from: https://www.ncbi.nlm.nih.gov/books/NBK144065/.

31. ASTM (2020). Standard tables for reference solar spectral irradiances: Direct normal and hemispherical on 37° tilted surface. https://www.astm.org/g0173-03r20.html. Accessed 23 March 2022.

32. McKenzie, R., Blumthaler, M., Diaz, S., Fioletov, V., Herman, J., Seckmeyer, G., Smedley, A., Webb, A. & New A (2014). Rationalizing nomenclature for uv doses and effects on joint publication of cie and wmo (World Meteorological Organization). CIE 209:2014, ISBN: 978-3-902842-35-0.

33. Kollias, N., Baqer, A. H., & Ou-Yang, H. (2003). Diurnal and seasonal variations of the UV cut-off wavelength and most

erythemally effective wavelength of solar spectra. *Photodermatology, Photoimmunology and Photomedicine, 19*(2), 89–92.

34. Perdiz, D., Grof, P., Mezzina, M., Nikaido, O., Moustacchi, E., & Sage, E. (2000). Distribution and repair of bipyrimidine photoproducts in solar UV-irradiated mammalian cells. Possible role of Dewar photoproducts in solar mutagenesis. *Journal of Biological Chemistry, 275*(35), 26732–26742.

35. Rochette, P. J., Therrien, J. P., Drouin, R., Perdiz, D., Bastien, N., Drobetsky, E. A., & Sage, E. (2003). UVA-induced cyclobutane pyrimidine dimers form predominantly at thymine-thymine dipyrimidines and correlate with the mutation spectrum in rodent cells. *Nucleic Acids Research, 31*(11), 2786–2794.

36. Han, W., & He, Y. (2009). Requirement for metalloproteinase-dependent ERK and AKT activation in UVB-induced G1-S cell cycle progression of human keratinocytes. *Photochemistry and Photobiology, 85*(4), 997–1003.

37. Ikehata, H., & Ono, T. (2011). The mechanisms of UV mutagenesis. *Journal of Radiation Research, 52*(2), 115–125.

38. Cohen, L., Brodsky, M. A., Zubair, R., Kohli, I., Hamzavi, I. H., & Sadeghpour, M. (2020). Cutaneous interaction with visible light: what do we know. *Journal of the American Academy of Dermatology*. https://doi.org/10.1016/J.JAAD.2020.03.115

39. Liebel, F., Kaur, S., Ruvolo, E., Kollias, N., & Southall, M. D. (2012). Irradiation of skin with visible light induces reactive oxygen species and matrix-degrading enzymes. *Journal of Investigative Dermatology, 132*(7), 1901–1907.

40. Tonolli, P. N., Chiarelli-Neto, O., Santacruz-Perez, C., Junqueira, H. C., Watanabe, I. S., Ravagnani, F. G., Martins, W. K., & Baptista, M. S. (2017). Lipofuscin generated by UVA turns keratinocytes photosensitive to visible light. *The Journal of Investigative Dermatology, 137*(11), 2447–2450.

41. Kim, S. J., Lee, H. J., Lee, J. H., Oh, H., Park, S., Lim, D. H., Park, M. S., & Lee, J. B. (2021). In vivo determination of the Infrared-A protection factor on human skin. *Skin Research and Technology, 27*(5), 814–823.

42. De Marais, T. L., Kluz, T., Xu, D., Zhang, X., Gesumaria, L., Matsui, M. S., Costa, M., & Sun, H. (2017). Transcription factors and stress response gene alterations in human keratinocytes following Solar Simulated Ultra Violet Radiation. *Scientific Reports, 7*(1), 1–13.

43. Zhang, X., Kluz, T., Gesumaria, L., Matsui, M. S., Costa, M., & Sun, H. (2016). Solar simulated ultraviolet radiation induces global histone hypoacetylation in human keratinocytes. *PLoS ONE, 11*(2), e0150175.

44. Lohan, S., Vitt, K., Scholz, P., Keck, C., & Meinke, M. (2017). ROS production and glutathione response in keratinocytes after application of β-carotene and VIS/NIR irradiation. *Chemico-biological Interactions, 28*, 01–07.

45. Schieke, S., Ruwiedel, K., Gers-Barlag, H., Grether-Beck, S., & Krutmann, J. (2005). Molecular crosstalk of the ultraviolet a and ultraviolet B signaling responses at the level of mitogen-activated protein kinases. *The Journal of Investigative Dermatology, 124*(4), 857–859.

46. Krutmann, J. (2006). The interaction of UVA and UVB wavebands with particular emphasis on signalling. *Progress in Biophysics and Molecular Biology, 92*(1), 105–107.

47. Jantschitsch, C., Majewski, S., Maeda, A., Schwarz, T., & Schwarz, A. (2009). Infrared radiation confers resistance to uv-induced apoptosis via reduction of DNA damage and upregulation of antiapoptotic proteins. *Journal of Investigative Dermatology, 129*(5), 1271–1279.

48. Portantiolo-Lettnin, A., Teixeira Santos Figueiredo Salgado, M., Gonsalez Cruz, C., Manoel Rodrigues da Silva Júnior, F., Cunha Gonzalez, V., de Souza Votto, A., Santos Trindade, G., & de Moraes Vaz Batista Filgueira, D. (2016). Protective effect of infrared-A radiation against damage induced by UVB radiation in

the melan-a cell line. *Journal of Photochemistry and Photobiology B, 163*, 125–132.

49. Worst, P. (2019). CsA is promoting tumor-like invasion in a long-term human skin equivalent. PhD thesis, Heinrich Heine University Düsseldorf, Germany. https://docserv.uni-duesseldorf.de/servlets/DocumentServlet?id=51883

50. Chiarelli-Neto, O., Ferreira, A. S., Martins, W. K., Pavani, C., Severino, D., Faiao-Flores, F., Maria-Engler, S. S., Aliprandini, E., Martinez, G. R., Di Mascio, P., Medeiros, M. H., & Baptista, M. S. (2014). Melanin photosensitization and the effect of visible light on epithelial cells. *PLoS ONE, 9*(11), e113266.

51. Lawrence, K. P., Douki, T., Sarkany, R. P. E., Acker, S., Herzog, B., & Young, A. R. (2018). The UV/visible radiation boundary region (385–405 nm) damages skin cells and induces "Dark" cyclobutane pyrimidine dimers in human skin in vivo. *Scientific Reports, 8*(1), 1–12.

52. Solmaz, H., Ulgen, Y., & Gulsoy, M. (2017). Photobiomodulation of wound healing via visible and infrared laser irradiation. *Lasers in Medical Science, 32*(4), 903–910.

53. De Jager, T. L., Cockrell, A. E., & Du Plessis, S. S. (2017). Ultraviolet light induced generation of reactive oxygen species. *Advances in Experimental Medicine and Biology, 99*, 615–623.

54. Petrocelli, T., Poon, R., Drucker, D. J., Slingerland, J. M., & Rosen, C. F. (1996). UVB radiation induces p21Cip1/WAF1 and mediates G1 and S phase checkpoints. *Oncogene, 12*(7), 1387–1396.

55. Bånrud, H., Stokke, T., Moan, J., & Berg, K. (1995). S phase arrest and induction of multinucleated cells after exposure to ultraviolet radiation. *Carcinogenesis, 16*(5), 1087–1094.

56. Runger, T. M., Farahvash, B., Hatvani, Z., & Rees, A. (2012). Comparison of DNA damage responses following equimutagenic doses of UVA and UVB: A less effective cell cycle arrest with UVA may render UVA-induced pyrimidine dimers more mutagenic than UVB-induced ones. *Photochemical and Photobiological Sciences, 11*(1), 207–215.

57. Lehman, T. A., Modali, R., Boukamp, P., Stanek, J., Bennett, W. P., Welsh, J. A., Metcalf, R. A., Stampfer, M. R., Fusenig, N., & Rogan, E. M. (1993). p53 mutations in human immortalized epithelial cell lines. *Carcinogenesis, 14*(5), 833–839.

58. Geyer, R. K., Nagasawa, H., Little, J. B., & Maki, C. G. (2000). Role and regulation of p53 during an ultraviolet radiation-induced G1 cell cycle arrest. *Cell Growth and Differentiation, 11*(3), 149–156.

59. De Laat, A., Van Tilburg, M., Van Der Leun, J. C., Van Vloten, W. A., & De Gruijl, F. R. (1996). Cell cycle kinetics following UVA irradiation in comparison to UVB and UVC irradiation. *Photochemistry and Photobiology, 63*(4), 492–497.

60. Dixon, R. J., Eperon, I. C., Hall, L., & Samani, N. J. (2005). A genome-wide survey demonstrates widespread non-linear mRNA in expressed sequences from multiple species. *Nucleic Acids Research, 33*(18), 5904–5913.

61. Athar, M., Kim, A. L., Ahmad, N., Mukhtar, H., Gautier, J., & Bickers, D. R. (2000). Mechanism of ultraviolet B-induced cell cycle arrest in G2/M phase in immortalized skin keratinocytes with defective p53. *Biochemical and Biophysical Research Communications, 277*(1), 107–111.

62. Berton, T. R., Pavone, A., & Fischer, S. M. (2001). Ultraviolet-B irradiation alters the cell cycle machinery in murine epidermis in vivo. *The Journal of Investigative Dermatology, 117*(5), 1171–1178.

63. Olsen, W. M., & Kirkhus, B. (1989). The epidermal cell kinetic response to ultraviolet B irradiation combines regenerative proliferation and carcinogen associated cell cycle delay. *Photochemistry and Photobiology, 50*(3), 391–397.

64. Olsen, W. M. (1988). Early cell kinetic effects of a single dose of monochromatic ultraviolet B irradiation on hairless mouse

epidermis. *The Journal of Investigative Dermatology, 91*(6), 585–589.

65. Tyagi, N., Bhardwaj, A., Srivastava, S. K., Arora, S., Marimuthu, S., Deshmukh, S. K., Singh, A. P., Carter, J. E., & Singh, S. (2015). Development and characterization of a novel in vitro progression model for UVB-induced skin carcinogenesis. *Scientific Reports, 5*(1), 1–11.

66. Hegedus, C., Boros, G., & Fidrus, E. (2020). PARP1 inhibition augments UVB-mediated. *Cancers, 12*(5), 1–29.

Authors and Affiliations

B. Plitta-Michalak[1,4] · N. Stricker[1] · E. Pavez Loriè[2,5] · I. Chen[3] · M. Pollet[2] · J. Krutmann[2] · B. Volkmer[3] · R. Greinert[3] · P. Boukamp[2] · A. Rapp[1]

1   Cell Biology and Epigenetics, Department of Biology, Technical University of Darmstadt, Schnittspahnstr. 10, 64287 Darmstadt, Germany

2   IUF-Leibniz Research Institute for Environmental Medicine, Auf'm Hennekamp 50, 40225 Düsseldorf, Germany

3   Centre of Dermatology, Elbe Clinics, Am Krankenhaus 1, 21614 Buxtehude, Germany

4   Present Address: Department of Chemistry, University of Warmia and Mazury in Olsztyn, Olsztyn, Poland

5   Present Address: Ludwig Boltzmann Institute for Traumatology, the Research Center in Cooperation with AUVA, Donaueschingenstraße 13, 1200 Vienna, Austria